Energy 142 (2018) 678–688

Contents lists available at ScienceDirect

Energy

journal homepage: www.elsevier.com/locate/energy

Online estimation of battery equivalent circuit model parameters and state of charge using decoupled least squares technique

Cheng Zhang*, Walid Allafi, Quang Dinh, Pedro Ascencio, James Marco

WMG, The University of Warwick, Coventry, CV4 7AL, United Kingdom

ARTICLE INFO

Article history:
Received 28 June 2017
Received in revised form
26 September 2017
Accepted 4 October 2017
Available online 11 October 2017

Keywords:
Equivalent circuit model
Recursive parameter estimation
SOC estimation
Decoupled least squares method

ABSTRACT

Battery equivalent circuit models (ECMs) are widely employed in online battery management applications. The model parameters are known to vary according to the operating conditions, such as the battery state of charge (SOC). Therefore, online recursive ECM parameter estimation is one means that may help to improve the modelling accuracy. Because a battery system consists of both fast and slow dynamics, the classical least squares (LS) method, that estimates together all the model parameters, is known to suffer from numerical problems and poor accuracy. The aim of this paper is to overcome this problem by proposing a new decoupled weighted recursive least squares (DWRLS) method, which estimates separately the parameters of the battery fast and slow dynamics. Battery SOC estimation is also achieved based on the parameter estimation results. This circumvents an additional full-order observer for SOC estimation, leading to a reduced complexity. An extensive simulation study is conducted to compare the proposed method against the LS technique. Experimental data are collected using a Li ion cell. Finally, both the simulation and experimental results have demonstrated that the proposed DWRLS approach can improve not only the modelling accuracy but also the SOC estimation performance compared with the LS algorithm.

1. Introduction

Battery energy storage systems are rapidly gaining popularity in high power and high voltage applications due to their advantageous features, such as high efficiency and low environmental impact when compared to fossil fuels. Among different battery types, Li ion batteries are typically the preferred power source to provide high power and energy density and long service life [1,2]. In order to maximize the battery performance, the key to success is an efficient battery model to support the system design, analysis and management strategies. Among existing battery model types, known as electrochemical models, reduced order models, and data-driven black-box models [3], equivalent circuit models (ECMs) offering acceptable modelling accuracy with ease of parametrization and implementation have been widely used for real-time battery management applications, including battery power prediction [4], state of charge (SOC) and state of health (SOH) estimation [5,6], balancing [7,8], charging control and optimization [9–11].

One of the challenges in utilizing an ECM is that the model parameters depend on the batteries' operating conditions, such as battery SOC, SOH and environmental temperature [12–16]. For example, the internal Ohmic resistance of a LiFePO4 cell and a Li ion NCA cell is almost doubled when the temperature decreases from 25°Cto0°C [13,14]. The dependency of the model parameters on the operating conditions can be captured using a look-up table, which is a widely employed technique for ECM parametrization [12–14,17]. However, it usually requires running a large number of experiments in order to collect sufficient test data to cover the entire range of the operating conditions to build the look-up tables. Another drawback is that the battery model parameters will change with ageing, making the previous characterization obsolete. Therefore, online recursive model parameter estimation algorithms are needed to solve this problem.

There are various methods within the literature for online recursive estimation of battery ECM parameters, such as recursive least squares (RLS) [18–20] and adaptive filter approaches [4,21–23]. Verbrugge et al. proposed using the weighted RLS (WRLS) method for online estimation of battery ECM parameters and SOC [18]. The authors then presented a new method in Ref. [19] to further improve the estimation performance by assigning each

* Corresponding author.
E-mail address: c.zhang.11@warwick.ac.uk (C. Zhang).

https://doi.org/10.1016/j.energy.2017.10.043

time-varying model parameter with one individual forgetting factor. These forgetting factors are optimized using the Newton's method. Guo et al. [20] used RLS for ECM parameter estimation and a Kalman filter (KF) for SOC estimation. Plett suggested a joint extended Kalman filter (EKF) [5] and a joint Unscented Kalman filter (UKF) [4] for the simultaneous estimation of the battery SOC and time-varying model parameters. A dual filter technique combining EKF and UKF was proposed in Ref. [23] to estimate together the ECM parameters and SOC. The performance of filter-based methods for SOC estimation depends on the availability of an accurate model and careful filter parameter tuning, e.g., to define the noise covariance. When using KF methods for joint estimation of parameters and states, the system order is usually high and the algorithm tuning can be difficult. In order to decouple the parameter identification and state estimation processes to suppress the cross interferences between these two parts, Wei et al. [24] proposed using the RLS method for recursive ECM parameter identification and the EKF method for SOC and SOH estimation.

Another difficulty for ECM parameter estimation is that the battery terminal voltage-current behaviours include both fast dynamics (FD), i.e., resistance and charge transfer effect, and very slow dynamics (SD), i.e., the diffusion effect. Consequently, the widely used LS methods, (e.g., RLS and WRLS) which estimate together all the model parameters suffer from numerical problems due to the high system stiffness, low data storage resolution and fast sampling [25,26]. Those effects were illustrated experimentally in Refs. [27–30]. In order to address this problem, Hu et al. [29] proposed a two-timescale scheme that estimates separately the battery FD and SD parameters. Here, the battery FD and SD were assumed to lie in different frequency ranges, and therefore they could be separated using linear high-pass and low-pass filters. The experimental results demonstrated modelling accuracy improvement of this two-timescale technique over the conventional WRLS method. However, this linear filter-based separation method is not a proper solution to deal with systems containing large nonlinearities and uncertainties that are common within battery models. Further, the SOC estimation logic was implemented in an open-loop manner and thus it could be sensitive to disturbances. Wei et al. [31] proposed a multi-timescale estimator to identify the ECM parameters and the battery open-circuit voltage (OCV) in real time. The parameters and OCV estimation processes were decoupled and implemented on different timescales to reduce the cross-interference between them. This leads to improved convergence and robustness. However, only first-order ECM was considered in Ref. [31], and the applicability of the proposed method for higher-order ECMs was not presented. Dai et al. [30] suggested a different method to estimate the battery FD and SD on separated time scales. In this study, the FD parameters were estimated using the RLS algorithm while the SD parameters were estimated using the EKF method. Although the modelling accuracy and parameter estimation consistency were illustrated through the experimental validation, the battery OCV and SOC were assumed to be known, which decreases the online applicability of this technique.

In order to address these problems, this paper presents a novel decoupled WRLS (DWRLS) method for online estimation of both the ECM parameters and battery SOC. The contributions of this paper are summarized as follows. First, based on a priori knowledge that the battery FD and SD occur on different timescales, the separation of them are implemented in time-domain in order to obviate the incorrect assumption of linear battery dynamics in the frequency domain. Second, the battery FD and SD parameters are estimated separately. When estimating the SD (or FD) part, the voltage response from the estimated FD (or SD) part is removed from the total model output voltage. By this way, the coupling between battery SD and FD can be effectively suppressed to improve the estimation performance. Third, the proposed algorithm can be implemented for batch data processing for offline model training, or operated recursively to estimate the ECM parameters in real time. Furthermore, this DWRLS approach can also be used for battery SOC estimation, which circumvents a full-order state observer to reduce the complexity. The SOC estimator is a closed-loop mechanism and is thus more robust against noises and external disturbances. Finally, test data are collected using a Li ion NCA cylindrical cell and comparative results are analysed to verify the algorithm's effectiveness.

The reminder of this paper is organized as follows. Section 2 presents the battery mathematical description, the LS algorithm and the proposed DWRLS scheme for online parameter estimation. Section 3 presents a simulation study to validate the performance of the proposed DWRLS method for parameter identification of a system that consists of both the FD and SD. Then the experimental test setup, the data acquisition and the offline model training results are introduced in Section 4. The recursive implementation of the DWRLS method for realtime parameter and SOC estimation, in comparison with the LS-based method, is demonstrated in Section 5. Concluding remarks and further work are given in Section 6.

2. Battery ECM formulation

2.1. ECM

The battery ECM is given in Fig. 1, where v, i are the battery terminal voltage and current, respectively. $v_j, j = 0, 1, 2$ is the overpotential voltage across R_j. The battery OCV depends on the SOC, i.e., $OCV = f(SOC)$. The OCV hysteresis is low and therefore negligible [28,32]. The resistors and capacitors $R_0, R_j, C_j, j = 1, 2$ are the time-varying model parameters that need to be identified. The total number of RC networks is regarded as the model order, which is a trade-off between model accuracy and complexity. For Li ion batteries, an ECM with two RC networks is commonly employed [13,14,27,29,30,33]. Let τ_1, τ_2 be the time constants of the two RC networks, and assume that $\tau_1 < \tau_2$. Herein, R_0, R_1, C_1 describe the battery resistance, charger transfer and double layer effect, which occur on a time scale of less than 10 s, and can be considered as the FD part. Meanwhile, R_2, C_2 are used to capture the battery diffusion effect occurring at a much larger time scale, typically around tens or hundreds of seconds, and therefore considered as the SD part [29,30]. The battery OCV also belongs to the battery SD since the battery SOC usually changes slowly within a standard drive cycle, that for example, represents urban vehicle driving [13,28,33].

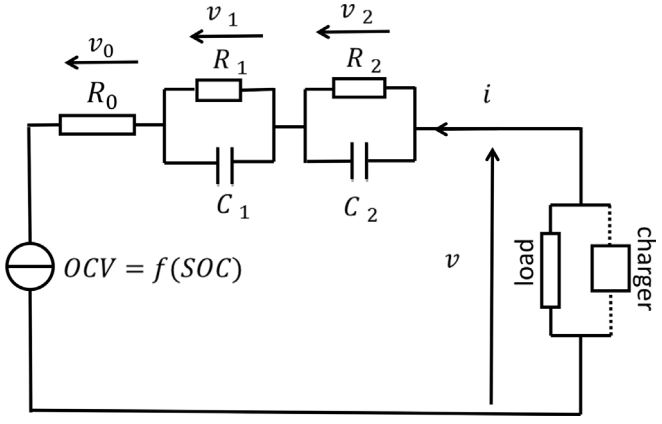

Fig. 1. Battery equivalent circuit model.

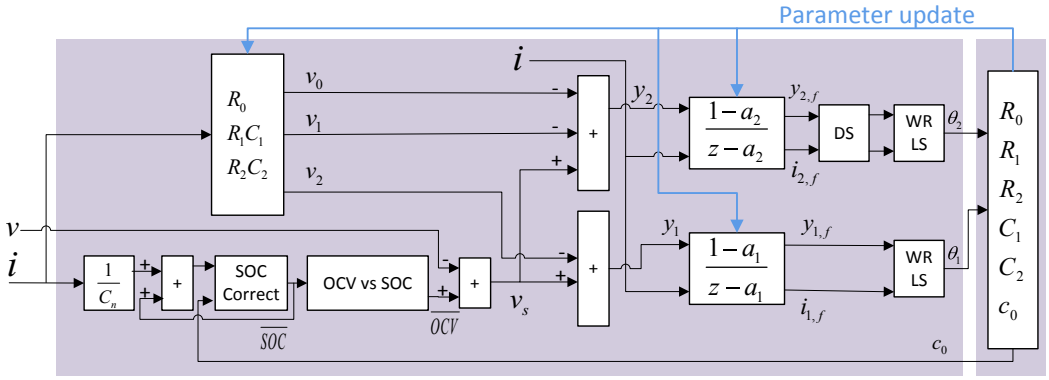

Fig. 2. Recursive implementation of the DWRLS method. The 'SOC correct' block stands for the SOC estimation algorithm given in Section 2.5. The 'DS' block stands for 'down-sample'.

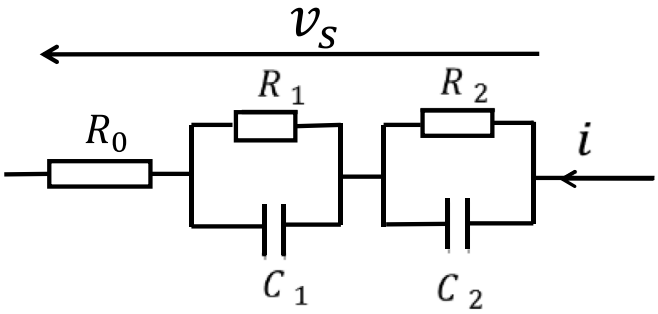

Fig. 3. Circuit model for the simulation study.

2.2. Problem formulation

It is assumed that the current between samples is constant. The dynamics of one RC network can be then given as follows:

$$v_j(k+1) = a_j v_j(k) + b_j I(k), \quad j = 1,2 \tag{1}$$

where

$$a_j = exp(-T_s/\tau_j)$$
$$b_j = R_j(1-a_j)$$

$v_j(k)$ stands for v_j at the k-th sampling time, and T_s is the sampling interval in seconds (s).

Let z be the time shift operator, i.e., $zx(k) = x(k+1)$. The z-transfer function from current i to v_j can then be expressed as

$$v_j(k) = \frac{b_j}{z-a_j} i(k)$$

The battery SOC is obtained using the widely employed coulomb counting method [5,33,34],

$$SOC(k+1) = SOC(k) + \frac{Ts}{C_n} I(k) \tag{2}$$

where $C_n$is the battery nominal capacity in Ampere-second (As).

Next, the model terminal voltage can be expressed as,

$$v(k) = OCV(k) + v_0(k) + v_1(k) + v_2(k) \tag{3}$$

Let v_s be the sum of the over-potentials across the resistors, one has:$v_s = v_0 + v_1 + v_2 = v - OCV$. If the battery SOC (and thus the OCV) is unknown, an estimated OCV value can be used instead, as follows,

$$v_s = v - \overline{OCV} = v - f\left(\overline{SOC}\right) \tag{4}$$

where $\overline{OCV}$ and $\overline{SOC}$ are the estimated battery OCV and SOC, respectively.

Combining Eq (3) and Eq (4) leads to,

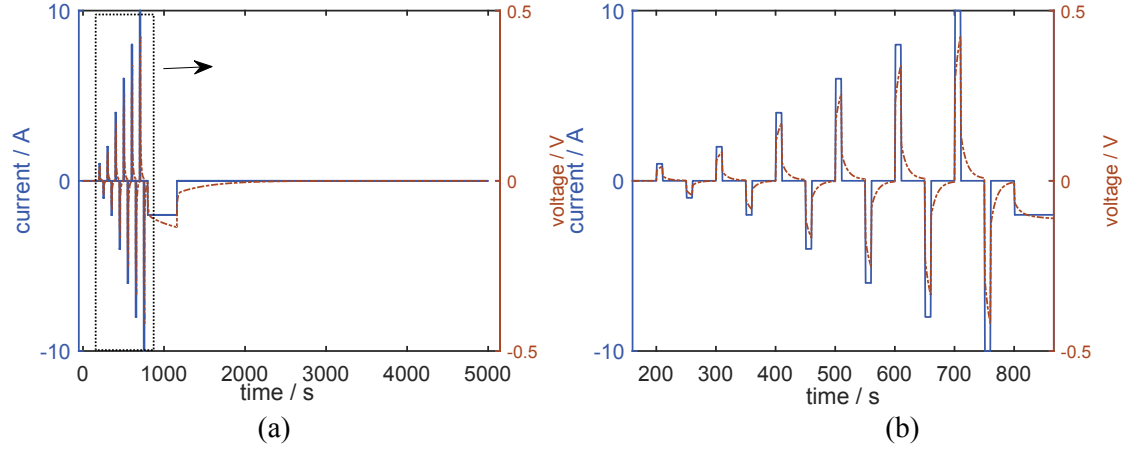

Fig. 4. The test data for the simulation study: (a) voltage $v_s$and current i; (b) a zoomed in segment.

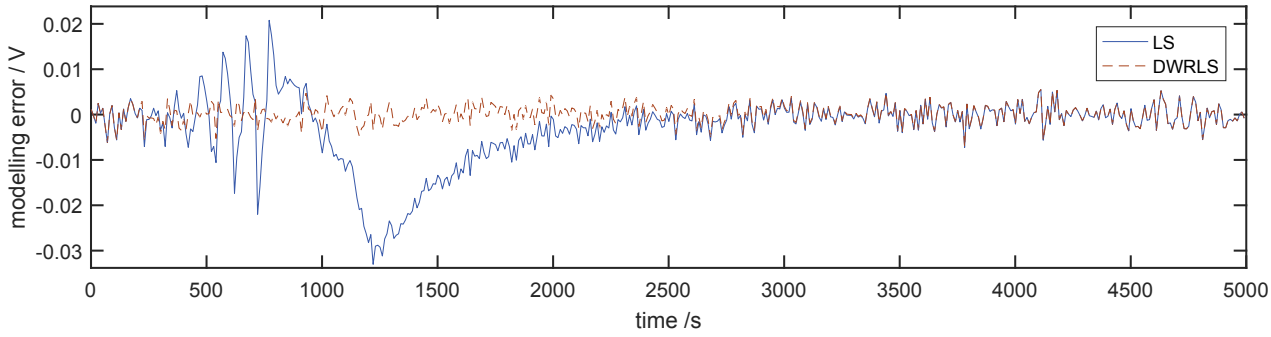

Fig. 5. Simulated modelling error using the LS method and the DWRLS method.

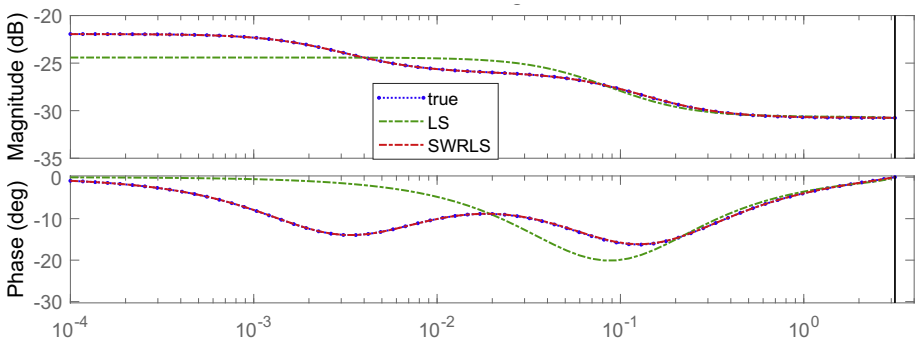

Fig. 6. Bode plots of the estimated models using the LS and DWRLS method (x-axis unit: rad/s).

$$v_s = v_0 + v_1 + v_2 + \left(OCV - \overline{OCV}\right) \tag{5}$$

Let $c_0 = OCV - \overline{OCV} = f(SOC) - f(\overline{SOC})$ as the OCV estimation error, which depends on the SOC estimation error and the slope of the OCV-SOC curve. If the battery SOC and $\overline{SOC}$ are both updated using Eq (2), the SOC estimation error will keep constant as the initial error, therefore c_0 depends on the slope of the OCV vs SOC curve alone and is slowly varying, as shown in Fig. 9. From Eq (5), we therefore get:

$$\begin{aligned} v_s(k) &= v_1(k) + v_2(k) + R_0 i(k) + c_0 \\ &= \left(R_0 + \frac{b_1}{z - a_1} + \frac{b_2}{z - a_2}\right) i(k) + c_0 \\ &= \frac{\theta_{n,2} z^2 + \theta_{n,1} z + \theta_{n,0}}{z^2 - \theta_{d,1} z - \theta_{d,0}} i(k) + c_0 \end{aligned} \tag{6}$$

where

$$\begin{aligned} \theta_{d,1} &= a_1 + a_2 \\ \theta_{d,2} &= a_1 a_2 \\ \theta_{n,2} &= R_0 \\ \theta_{n,1} &= b_1 + b_2 - R_0(a_1 + a_2) \\ \theta_{n,0} &= R_0 a_1 a_2 - a_2 b_1 - a_1 b_2 \end{aligned}$$

2.3. LS and RLS formulation

This section presents the established LS and RLS mechanisms for battery ECM parameter estimation. The regression form of Eq (6) can be expressed as:

$$\begin{aligned} z^2 v_s(k) = {} & \theta_{d,1} z v_s(k) + \theta_{d,0} v_s(k) + \theta_{n,2} z^2 i(k) + \theta_{n,1} z i(k) + \theta_{n,0} i(k) \\ & + (1 - \theta_{d,1} - \theta_{d,0}) c_0 \end{aligned} \tag{7}$$

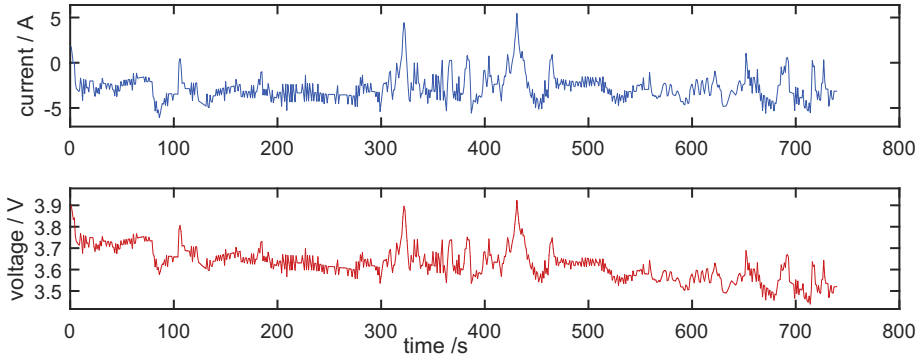

Fig. 7. Battery motorway drive cycle test starting from 75% to 60% SOC at 25.°C.

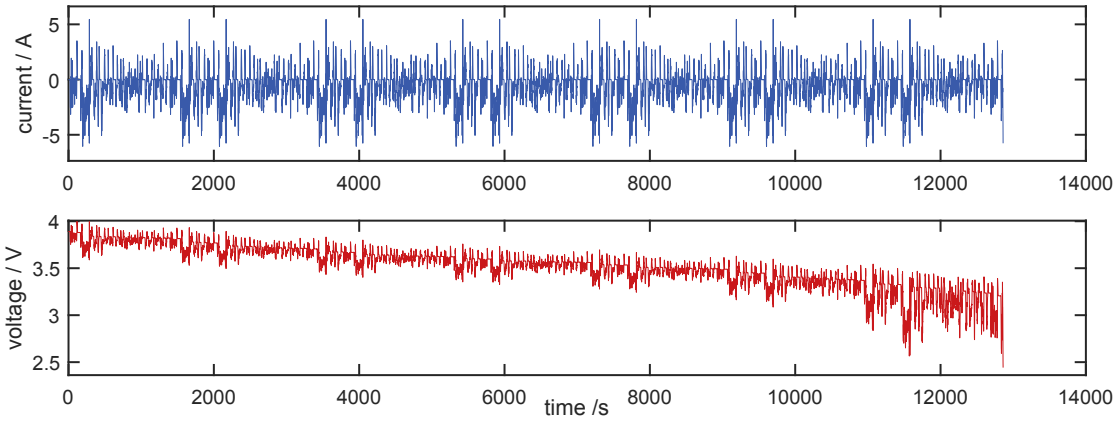

Fig. 8. Battery urban drive cycle test starting from 75% SOC at 25.°C.

Let

$$y(k) = z^2 v_s(k),$$
$$\theta = [\theta_{d,1}, \theta_{d,0}, \theta_{n,2}, \theta_{n,1}, \theta_{n,0}, (1-\theta_{d,1}-\theta_{d,0})c_0]^T,$$
$$\phi(k) = \left[z v_s(k), v_s(k), z^2 i(k), z i(k), i(k), 1\right]^T$$

Eq. (7) can be re-expressed as

$$y(k) = \theta^T \phi(k) \tag{8}$$

The model parameters are obtained by minimizing a cost function of

$$J_{LS} = \sum \left[y(k) - \theta^T \phi(k)\right]^2 \tag{9}$$

Eq (8) is the linear-in-the-parameter formulation, and therefore after obtaining i, v_s (and thus$y(k), \phi(k)$), the unknown parameter θ can be obtained using LS algorithm in Eq (10), or recursively using RLS or WRLS algorithm in Eq (11).

$$\theta = \left(\Phi^T \Phi\right)^{-1} \Phi^T Y$$
$$\Phi = [\phi(1), \phi(2), \ldots, \phi(N)]^T,$$
$$Y = [y(1), y(2), \ldots, y(N)]^T \tag{10}$$

where$N$ is the total number of data samples.

$$\begin{aligned} e(k+1) &= y(k+1) - \phi^T(k+1)\theta(t) \\ \theta(k+1) &= \theta(k) + P(k+1)\phi(k+1)e(k+1) \\ P(k+1) &= P(k) - \frac{P(k)\phi(k+1)\phi^T(k+1)P(k)}{1+\phi^T(k+1)P(k)\phi(k+1)} + Q_0 \end{aligned} \tag{11}$$

Q_0 is a small positive-definite matrix introduced to prevent the covariance matrix $P$from keeping decreasing and eventually losing the parameter tracking capability. The initial parameters $\theta(0), P(0)$ can be obtained using priori knowledge, or by performing a block-wise LS estimation as discussed within [35,36].

The implementation procedure of the LS method in Eq (10) is summarized in Table 1 for completeness.

The implementation procedure of the RLS method in Eq (11) is well documented in a number of research publications and educational texts, such as [35,36], and is therefore not discussed in detail here.

2.4. DWRLS method

The previous section presents the classical LS-based method for battery ECM parameter estimation. The challenge is that the algorithm's numerical stability and parameter convergence depend on the selection of the sampling interval [25,27,37]. Since the battery system consists of both FD and SD, if the sampling rate is high, the pole of the SD part lies closely to the unit circle, and its estimation may even become unstable in the presence of system uncertainties and noises. On the other hand, if the sampling rate is too slow, the FD part can be lost due to aliasing. For example, suppose $\tau_1 = 10s$ and $\tau_2 = 400s$ in the ECM in Fig. 1. As a rule of thumb$T_s/\tau_1 < 0.5$,

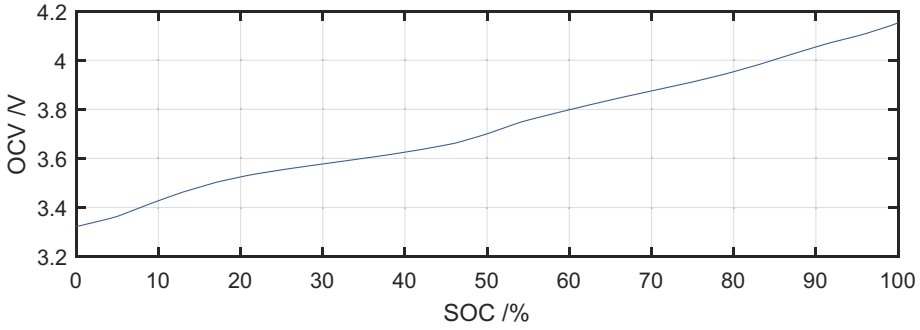

Fig. 9. Battery OCV versus SOC.

Table 1
The implementation procedure of the LS method.

Step 1: collect battery terminal voltage and current measurements $v(k), i(k),\ k = 0 : N$
Step 2: estimate initial SOC, i.e., $\overline{SOC}(0)$
Step 3: calculate $\overline{SOC}(k), k = 1 : N$ using Eq (2)
Step 4: obtain $\overline{OCV}(k)$ using $\overline{SOC}(k)$.
Step 5: calculate $v_s(k)$ in Eq (4), and thus obtain $y(k), \phi(k)$
Step 6: calculate θ (and thus the model parameters a_j, b_j, R_0, c_0) using Eq (10)

such that $T_s < 5s$. Suppose $T_s = 2s$, the SD pole is then located close to the unit circle, i.e., $a_2 = \exp(-T_s/\tau_2) = 0.995$. Further, when the FD and SD parameter are together estimated using the LS method, the estimation is normally biased towards the high frequency range. This leads to poor accuracy within the low frequency domain. The LS method is thus also sensitive to high frequency noise and disturbances [27–29]. As illustrated in Ref. [27], the modelling performance of the discrete time domain RLS method decreases with fast sampling data. The DWRLS method is proposed here to address these problems.

Consider the objective function for the ECM model parameter optimization as

$$J = \sum_k e^2(k) \tag{12}$$

where $e(k) = v_s - v_0(k) - v_1(k) - v_2(k) - c_0$ is the modelling error.

Let

$$\begin{aligned} y_1(k) &= v_s(k) - v_2(k) \\ y_2(k) &= v_s(k) - v_0(k) - v_1(k) \end{aligned} \tag{13}$$

where y_1 corresponds to the battery FD voltage (i.e. $y_1 = v_0 + v_1 + c_0$), because the SD voltage v_2 is subtracted from the total model output v_s. Similarly, y_2 represents the battery SD voltage. The cost function in Eq (12) is re-expressed as follows,

$$\begin{aligned} J &= \sum [y_1(k) - v_0 - v_1(k) - c_0]^2 \triangleq J_1, \\ J &= \sum [y_2(k) - v_2(k) - c_0]^2 \triangleq J_2 \end{aligned} \tag{14}$$

Here, J_1 and J_2 are the sub-cost functions corresponding to the battery FD and SD, respectively. The minimization processes of J_1 and J_2 can be iteratively implemented. The key concept is that when R_0, R_1, C_1 are estimated by minimizing J_1, R_2, C_2 are assumed to be known to calculate v_2 using Eq (1) and then subtract it from v_s. Similarly, when estimating R_2, C_2, c_0 by minimizing J_2, keep $R_0, R_1 C_1$ constant. The simulated over-potentials across the resistors, i.e., v_0, v_1, v_2, are used to link the two identification parts of the method together to form the complete model.

For the SD identification, the objective function is:

$$J_2 = \sum [y_2(k) - v_2(k) - c_0]^2 = \sum \left[y_2(k) - \frac{b_2}{z - a_2} i(k) - c_0 \right]^2 \tag{15}$$

The LS algorithm presented in Section 2.3 can be used to find the parameters a_2, b_2, c_0 in Eq (15) by minimizing:

$$\begin{aligned} \bar{J}_2 &= \sum [z y_2(k) - a_2 y_2(k) - b_2 i(k) - (1 - a_2) c_0]^2 \\ &= \sum \left[p_2(k) - \theta_2^T \phi_2(k) \right]^2 \end{aligned}$$

where $p_2(k) = z y_2(k), \phi_2(k) = [y_2(k), i(k), 1]^T$ and $\theta_2 = [a_2, b_2, (1 - a_2) c_0]^T$

However, note that

$$\bar{J}_2 = \sum (z - a_2)^2 \left[y_2(k) - \frac{b_2}{z - a_2} i(k) - c_0 \right]^2 = (z - a_2)^2 J_2 \tag{16}$$

Since $(z - a_2)^2$ is a high pass filer, the parameter estimation by minimizing $\bar{J}_2$ will be biased towards the high frequency domain. To avoid this, the test data can be pre-processed using a low pass filter of the form $\frac{1 - a_2}{z - a_2}$,

$$\begin{aligned} y_{2f}(k) &= \frac{1 - a_2}{z - a_2} y_2(k),\ i.e.,\ y_{2f}(k+1) = a_2 y_{2f}(k) + (1 - a_2) y_2(k) \\ i_{2f}(k) &= \frac{1 - a_2}{z - a_2} i(k),\ i.e.,\ i_{2f}(k+1) = a_2 i_{2f}(k) + (1 - a_2) i(k) \end{aligned} \tag{17}$$

A new objective function given below can be then minimized to obtain the SD parameters,

$$\begin{aligned} \bar{J}_{2f} &= \sum \left[z y_{2f}(k) - a_2 y_{2f}(k) - b_2 i_{2f}(k) - c_0 \right]^2 \\ &= \sum \left[p_{2f}(k) - \theta_{2f}^T \phi_{2f}(k) \right]^2 \end{aligned} \tag{18}$$

where $p_{2f}(k) = z y_{2f}(k)$, $\phi_{2f}(k) = [y_{2f}(k), i_{2f}(k), 1]^T$ and $\theta_{2f} = [a_2, b_2, (1 - a_2) c_0]^T$

The same method can be applied for the FD identification, i.e., by minimizing J_1 to obtain a_1, b_1, R_0,

$$\begin{aligned} y_{1f}(k) &= \frac{1 - a_1}{z - a_1} y_1(k),\ \text{i.e.,}\ y_{1f}(k+1) = a_1 y_{1f}(k) + (1 - a_1) y_1(k) \\ i_{1f}(k) &= \frac{1 - a_1}{z - a_1} i(k),\ \text{i.e.,}\ i_{1f}(k+1) = a_1 i_{1f}(k) + (1 - a_1) i(k) \end{aligned} \tag{19}$$

$$\begin{aligned} \bar{J}_{1f} &= \sum \left[z y_{1f}(k) - a_1 y_{1f}(k) - R_0 (z - a_1) i_{1f} - b_1 i_{1f}(k) - c_0 \right]^2 \\ &= \sum \left[p_{1f}(k) - \theta_{1f}^T \phi_{1f}(k) \right]^2 \end{aligned} \tag{20}$$

where $p_{1f}(k) = z y_{1f}(k)$, $\phi_{1f}(k) = [y_{1f}(k), z i_{1f}(k), i_{1f}(k), 1]^T$ and $\theta_{1f} = [a_1, R_0, b_1 - a_1 R_0, (1 - a_1) c_0]^T$

The filters designed in Eqs (17) and (19) are based on the approximate maximum likelihood principle detailed in Refs. [38,39], which is a simple and useful model identification technique. Another benefit of using this kind of filters is to suppress the high frequency disturbances due to noises or un-modelled dynamics. Further, it can be shown that $\bar{J}_{2f} = J_2$, and $\bar{J}_{1f} = J_1$. Therefore, although the battery FD and SD parts are identified separately, the original model training criteria, i.e., the cost function in Eq (12), is unmodified, since $J_1 = J_2 = J$. The overall modelling accuracy can thus be secured when combining the SD and FD parts to form the complete model. Finally, since $\frac{1 - a_2}{z - a_2}$ is a low pass filter and J_{2f} corresponds to the battery SD, the filtered data y_{2f}, i_{2f} can be down-sampled to reduce the computational complexity and to improve the numerical stability without loss of information [29].

Eventually, the decoupling between the battery FD and SD voltage responses is performed in a twofold manner, i.e., the subtraction separation in Eq (13) and the low pass filtering in Eq (17). Another useful technique to further reduce the interference between the SD and FD parts is to use a short data length for the FD

estimation, since a short data length can still consist of sufficient information about the FD part, while the SD part is not fully excited.

However, there is an implementation issue with this filter design, since a_1, a_2 are unknown before the identification process is conducted. To overcome this problem, the algorithm can be executed in an iterative manner [38]. For each iteration, the a_1, a_2 obtained from the previous iteration can be used to construct the filters. The parameter initialization can be realized using prior knowledge, or a look-up table trained offline.

The implementation procedure of the DWRLS method for offline model training by processing batch data is given in Table 2.

2.5. SOC estimation

Note that $c_0(k) = OCV(k) - \overline{OCV}(k)$. Therefore, when c_0 is estimated, the battery OCV and SOC estimation can be compensated as follows

$$\begin{aligned} \overline{OCV}_{correction} &= \overline{OCV}(k) + c_{correction} \\ \overline{SOC}_{correction} &= f^{-1}\left(\overline{OCV}_{correction}\right) \end{aligned} \tag{21}$$

where f^{-1} stands for the inverse of $f(\overline{SOC})$ in (4) and obtained from the battery OCV vs SOC relationship, and

$$c_{correction} = \frac{1}{N_1}\sum_{L=1}^{N_1} c_0(k-L+1)$$

As discussed within [28], there is no need to correct the SOC estimation at every sample, since it generally takes some time for the estimates to converge to stable values. Therefore, this SOC correction approach is executed every N_1 samples to avoid estimation fluctuations. Note that this SOC estimation only affects the $c_0$in the parameter estimation process. Therefore, reset $c_0(k)$ to $c_0(k) - c_{correction}$ in the estimated $\theta_{1,f}^T, \theta_{2,f}^T$ after each SOC correction, and the rest model parameters R_0, a_j, b_j will then remain unaffected [28].

The DWRLS method for both parameter and SOC estimation can be implemented in a recursive manner for online applications, as illustrated in Fig. 2.

3. Simulation study

This section presents a simulation study to show the efficacy of the proposed DWRLS method for the offline identification of a 2nd order linear system which consists of both FD and SD.

3.1. Simulation set up

Consider only the RC networks and R_0 in the ECM as the system to be identified, as shown in Fig. 3. The system parameters are given below in Eq (22),

Table 2
The implementation procedure of the DWRLS method for offline model training.

Initialize$a_1, b_1, a_2, b_2, R_0, \overline{SOC}(0)$
For each iteration
Step 1 calculate $\overline{SOC}(k), \overline{OCV}(k)$and then $v_s(k)$, $k = 1:N$
Step 2 calculate $v_1(k), v_2(k)$, $k = 1:N$using Eq (1)
Step 3 calculate $y_1(k), y_2(k)$, $k = 1:N$using Eq (13)
Step 4 calculate $y_{1,f}(k), y_{2,f}(k), i_{1,f}(k), i_{2,f}(k)$, $k = 1:N$ using Eq (17) and Eq (19)
Step 5 estimate $\theta_{2,f}^T$in Eq (18) and $\theta_{1,f}^T$in Eq (20), using the LS method

$$\tau_1 = 10s,\ \ \tau_2 = 400s,\ \ R_1 = 0.02\Omega,\ \ R_2 = 0.03\Omega,\ \ R_0 = 0.03\Omega \tag{22}$$

The load current simulates the hybrid pulse power test, which is widely used for battery characterization [14,27]. The current i and the over-potential $v_s$are shown in Fig. 4(a). The current profile consists of six pulse current tests, followed by a 360 s constant current (2 A) discharge and a rest period for approximately 1 h. Each pulse current test consists of 10-s charging and 10 s discharging, and the pulse current levels are 1, 2, 4, 6, 8 and 10 A, in sequence. The rest period between any two consecutive pulses is 40 s. Fig. 4(b) shows a zoomed-in segment of the load current. The sampling time is 1 s.

The current and voltage signals are corrupted with white Gaussian noise, and the root mean square (RMS) of the noise values are 10 mA and 2 mV, respectively, representing the low noise level.

The two parameter identification methods, the LS and DWRLS represented in Tables 1 and 2 respectively, are selected for the comparative study. For the DWRLS approach, the total iteration number is set to 3, as it will be shown in the following section that the parameter estimation has converged at the second iteration.

The initial model parameters are set as $\tau_1 = 20s,\ \tau_2 = 200s,\ R_1 = 0.01\Omega,\ R_2 = 0.01\Omega,\ R_0 = 0.02\Omega$ for the DWRLS method. Note that for the SD identification, all the 5000 sample data set is used; while for the FD identification, a smaller data set, i.e., 400 data samples starting from the first current pulse, is used to further decrease the interferences from the SD part, as explained in Section 2.4.

3.2. Simulation results and discussion

The parameters obtained using the LS method are

$$\tau_1 = 16.6s,\ \ a_2 = -0.44,\ \ R_1 = 0.0298\Omega,\ \ R_2 = 0.00022\Omega,\ \ R_0 = 0.03\Omega$$

Because $a_2 = -0.44$and $a_2 = \exp(-T_s/\tau_2)$, the second RC network time constant τ_2 becomes an imaginable number. Further, because $R_2$is much smaller thanR_0, R_1, the voltage contribution from the second RC network is also negligible. The estimated parameters using the LS algorithm diverge away from the true parameters in Eq (22), and the 2nd RC network of the system (i.e., the SD part) is not captured.

The parameter identification results using the DWRLS approach at each iteration are given in Table 3. It can be seen that the estimated parameters using the DWRLS method converge toward the true parameters in Eq (22) and are significantly better than those of the LS method. Table 3 also shows that the DWRLS algorithm can give the good estimation directly after the first iteration from the incorrect initial estimates. This therefore can validate the convergence rate of the proposed technique.

Next, the modelling errors ($e(k)$ defined in Eq (12)) using the LS and DWRLS schemes are described in Fig. 5. As it can be seen, the DWRLS mechanism achieves better modelling accuracy than the one obtained by using the LS approach. The RMS errors (RMSEs) are

Table 3
The parameter identification results using the DWRLS method at each iteration.

Iteration No.	τ_1	τ_2	R_1	R_2	R_0
Initialization	20	200	0.01	0.01	0.02
Iteration 1	10.55	425	0.0206	0.0301	0.030
Iteration 2	10.20	406	0.0201	0.0300	0.030
Iteration 3	10.16	404	0.0202	0.0300	0.030

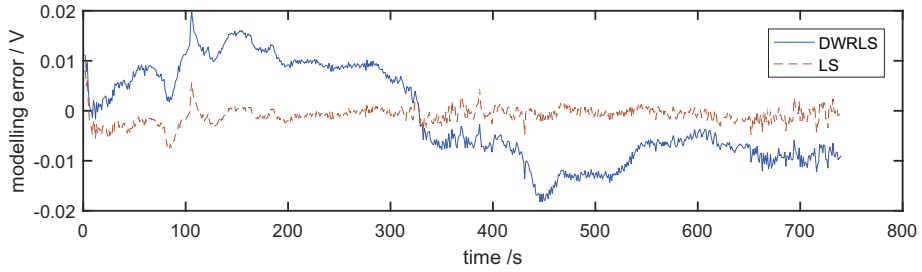

Fig. 10. Modelling error comparison between LS and DWRLS method for offline model estimation.

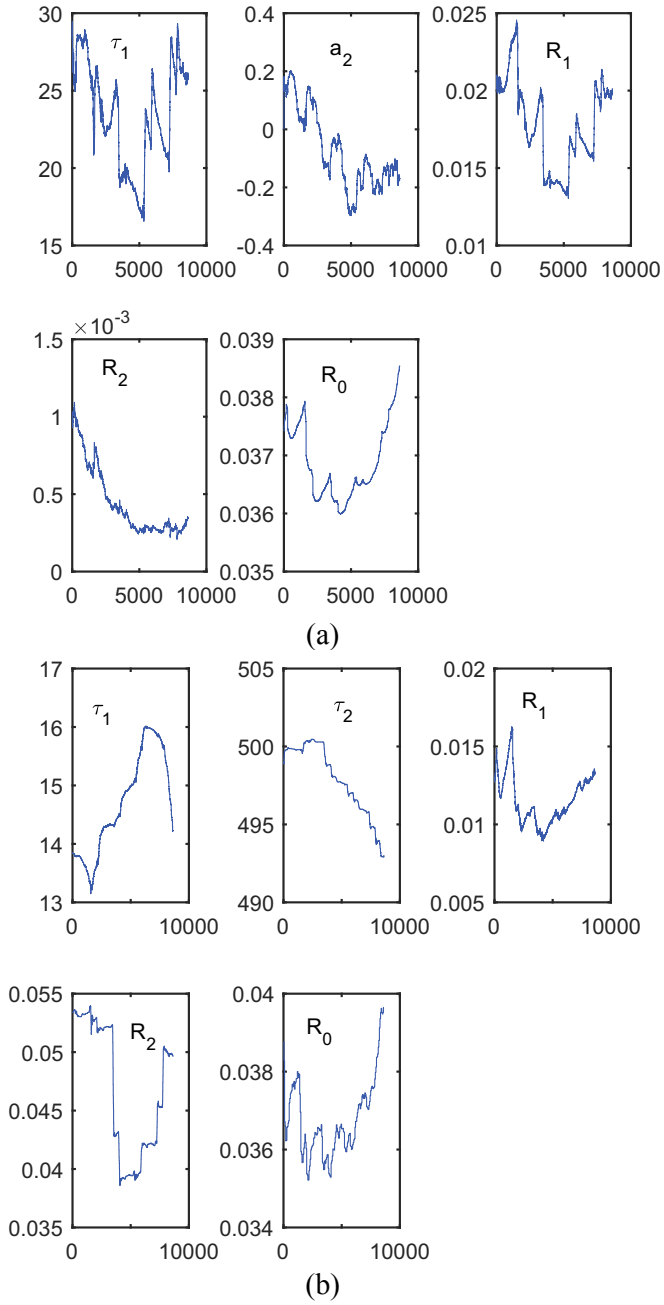

Fig. 11. The parameter estimation results using the LS method (a) and the DWRLS method (b). The x-axis unit is time in seconds. For the LS results, a_2 is given instead of τ_2, since when $a_2 < 0$, τ_2 becomes a complex number.

2 mV and 7.9 mV, respectively. The model identified by the LS method causes the large transient errors as the current changes and the large bias error when the current keeps constant (i.e., low frequency excitation signal) due to the model discrepancy. A Bode plot of the two identified models are shown in Fig. 6, which shows that both the LS and DWRLS methods can achieve high accuracy at high frequency range (>0.5 rad/s). However, the LS estimation shows the noticeable bias error in the low frequency domain (<0.06 rad/s), while the DWRLS estimation still maintains the high accuracy.

4. Offline ECM parameter identification

This section presents a comparative study between the classical LS method and the DWRLS method for offline ECM parameter identification using experimental test data.

4.1. Experimental test setup

Experimental data have been collected from a commercial cylindrical 3 A h 18650-type cell which comprises graphite negative electrode and a $LiNiCoAlO_2$ positive electrode. A Bitrode battery cycler is used with a thermal chamber for maintaining the ambient temperature constant at 25 °C. First, the battery is fully charged by the constant-current, -constant-voltage (CC-CV) method, and then discharged at 1C rate to 75% SOC, followed by a rest period of 2 h. Finally, a drive cycle test that simulates a motorway driving scenario is applied until the battery reaches the cut-off voltage at 2.5 V. The test data from 75% to 60% SOC are used in this section as presented in Fig. 7. The sampling time is 1 s.

Another drive cycle test is implemented in the same way, which simulates an urban driving scenario starting from 75% SOC until end of discharge, as depicted in Fig. 8.

The battery OCV versus SOC relationship is characterized experimentally [32], as given in Fig. 9.

4.2. Offline model training results and discussion

The motorway-drive test data in Fig. 7 are used here for offline model estimation. Since SOC does not show a significant change and the temperature is kept constant, the model parameters are assumed to keep constant [13]. In this section, the battery SOC is assumed to be known. Therefore, the OCV can be obtained using the OCV-SOC relationship defined in Fig. 9, and then subtracted from the battery terminal voltage response. Similar to Section 3.2, for the DWRLS method, all the data samples are used for the SD part identification; while for the FD part identification, only the first 400 data samples are used.

The identified model parameters by the LS method are given below.

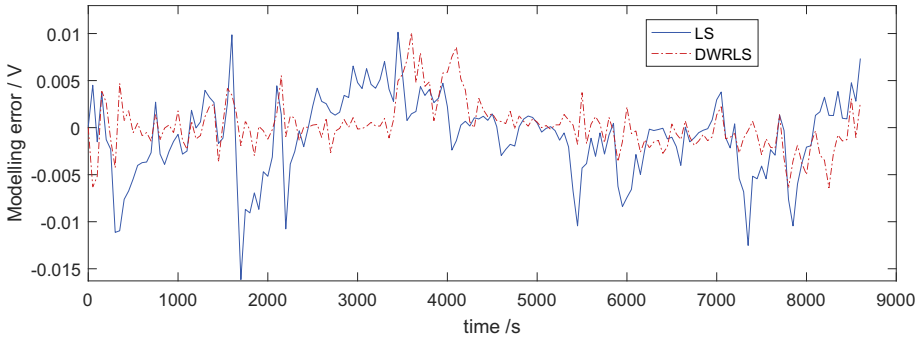

Fig. 12. Modelling error using the LS and DWRLS methods.

$\tau_1 = 34.5s,\ a_2 = -0.023,\ R_1 = 0.0252\Omega,\ R_2 = 0.00037\Omega,\ R_0 = 0.0355\Omega$

Note that the model has a negative pole a_2, corresponding to an imaginary time constant of the 2nd RC networks. Once again similar to the LS results in Section 3.2, R_2 is very small, and the voltage contributions of the 2nd RC networks v_2 is negligible compared withv_0, v_1.

The identified model parameters using the DWRLS method are

$\tau_1 = 19s,\ \tau_2 = 423s,\ R_1 = 0.0132\Omega,\ R_2 = 0.0157\Omega,\ R_0 = 0.0354\Omega$

The modelling errors using the two schemes are compared in Fig. 10. The results indicate that the LS method shows biased modelling error, and its performance is much less efficient than the DWRLS method. The modelling RMSEs are in turn 9.4 mV and 1.9 mV. Therefore, it can be concluded that the proposed technique can improve the modelling accuracy. Further, from the two identified model parameter sets, it can also be observed that the DWRLS model covers a wider timescale (the larger RC time constant is 423 s) than the LS one (the larger RC time constant is 34.5 s).

This section gives similar parameter estimation results to the simulation study in Section 3.2. Therefore, we can reasonably assert that similar conclusions apply here, i.e., that the identified model using the DWRLS method offers better modelling accuracy in the low frequency range than the LS method.

5. Realtime parameter and SOC estimation

This section presents a comparative study of the realtime parameter and SOC estimation results using the recursive implementation of the LS and DWRLS schemes. The urban drive cycle test data in Fig. 8 from 75% to 25% SOC are used here. The test data below 25% SOC are discarded in order to circumvent the nonlinear battery dynamics in the low SOC range. The estimated initial SOC is assumed to be 65%, with a 10% error.

The parameter estimation results using the LS and DWRLS methods are shown in Fig. 11. As it can be seen, both the two techniques show noticeable parameter variations as the SOC decreases from 75% to 25% SOC. The ECM parameter evolution can affect the battery terminal voltage dynamics and the power capacity (due to the perceived resistance changes), which needs to be taken into consideration for online battery management. Note also that the results of the two methods both indicate that the battery internal resistance is relatively lower at around 50% SOC. Moreover, since the twoR_0estimations are similar, it can be concluded that the both LS and DWRLS methods can estimate accurately the series resistanceR_0.

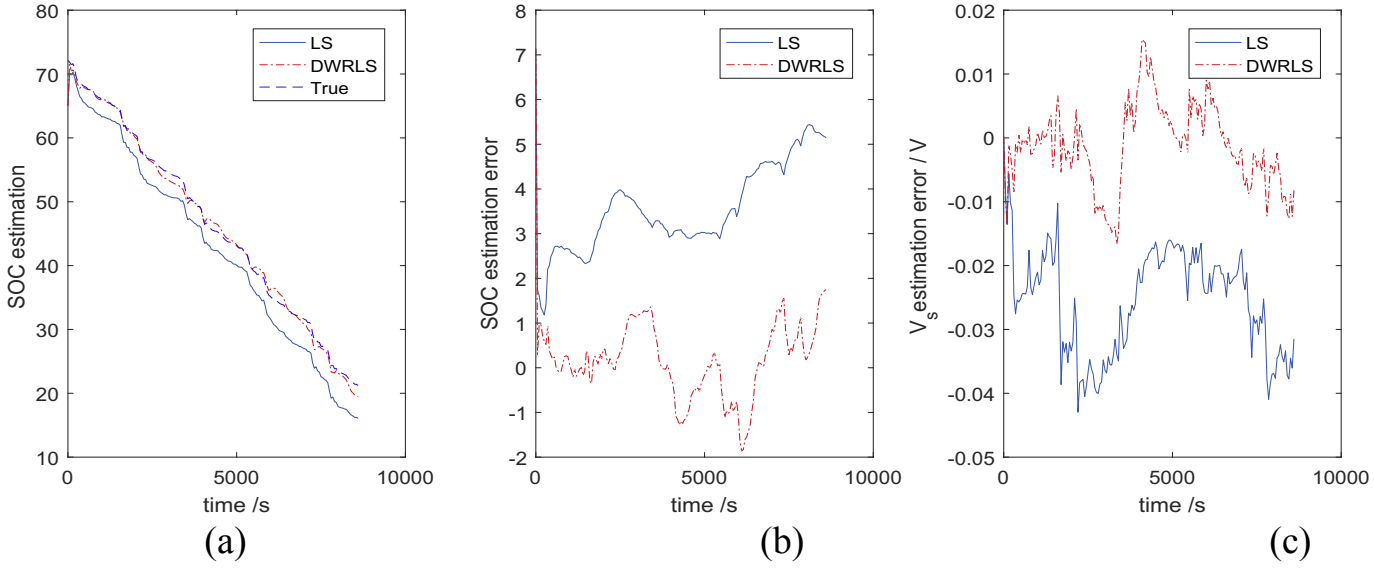

Fig. 13. SOC estimation results.

The two RC network time constants obtained using the DWRLS algorithm are widely separated in timescale, and the two resistors are both noticeable. On the other hand, the second RC network identified by the LS algorithm only corresponds to high frequency fluctuations, and its voltage contribution to the total model output is negligible. Furthermore, the DWRLS model covers a wider timescale than the LS model. The parameter estimation results of the LS method, i.e., the two pole locations, are similar to those presented in Section 3.2 and Section 4.2.

The modelling errors are analysed in Fig. 12. As it can be seen, the DWRLS model shows the better accuracy over the LS model. The modelling RMSEs are 2.8 mV and 4.4 mV, respectively. The low modelling errors come as no surprise because of the adaptive nature of the two algorithms, which can keep track of the model parameter evolutions as the SOC decreases to improve the modelling accuracy.

Next, the SOC estimation using the comparative tools is carried out and the results are plotted in Fig. 13. As it can be seen, the SOC estimation accuracy of the DWRLS method is remarkably better than that of the LS method. The SOC RMSEs are 0.86% and 2.98%, respectively. This result can be explained by the difference of the-$v_s$estimations error, i.e., $v_s(true) - v_s(estimation)$, using the two methods, as shown in Fig. 13(c). $v_s(true)$ is calculated by subtracting the true OCV from the measured voltage, i.e., $v_s(true) = v - OCV$, and $v_s(estimation)$is a sum of the model's simulated over-potentials across the resistors, i.e., $v_s(estimation) = v_0 + v_1 + v_2$. During the charging/discharging operation, the battery OCV is not measurable, and can only be estimated by subtracting the over-potentialv_s (which depends on the model parameter identification) from the measured battery terminal voltage, i.e., $OCV = v - v_s$. Therefore, the better parameter identification scheme can improve the estimation accuracy of the over-potentialv_s, and subsequently improve the OCV and SOC prediction performances. As depicted in Fig. 13(c), the v_s estimation error using the LS algorithm is higher than that of the DWRLS algorithm. Subsequently, the OCV estimation error of the LS model is also higher, leading to the larger SOC bias error as depicted in Fig. 13(b). Based on the conclusions from Section 3 and Section 4, we can reasonably assert that this poor SOC estimation performance of the LS algorithm is caused by the model discrepancy in the low frequency domain, and this problem can be overcome by the proposed DWRLS technique.

6. Conclusion

6.1. Discussion and future work

Previous work in the literature has already established the necessity of realtime estimation of the time-varying ECM parameters in order to improve the SOC prediction accuracy [18,20,24,40]. The results and analysis presented in the previous sections in this paper have already demonstrated the superiority of the proposed method over the conventional LS based approaches as the benchmark. Another advantage of this DWRLS method, compared against the methods combining RLS and KF as in Refs. [20,24], is that the proposed algorithm does not require an additional full-order observer (i.e., KF) for SOC estimation. The SOC estimation accuracy of the DWRLS method is about 1%, which is comparable with the previously reported results in Refs. [20,24,33].

The proposed DWRLS method for adaptive ECM parameter identification considers only the estimation of the resistance and capacitance values, and depends on the knowledge of the battery OCV vs SOC relationship, which can be characterized offline experimentally [32]. However, the OCV-SOC relationship also changes with temperature and ageing [41,42]. The temperature effect on battery OCV is negligible for the Li ion NCA cell used in this paper (the OCV varies less than 5 mV when the temperature decreases from $25^{\circ}C$ to $0^{\circ}C$ according to our test results). Ageing can also cause OCV variations, which need to be taken into consideration in order to further improve SOC estimation accuracy. A scheme to update the OCV-SOC relationship as the battery ages is needed, and will be investigated in future work.

6.2. Concluding remarks

ECMs are widely used in battery management system applications, and the model parameters depend on the operation conditions. Adaptive parameter estimation techniques can be used to track the parameter evolution and to improve the modelling accuracy. In addition, the battery system consisting of both fast and slow dynamics causes numerical problems to the traditional LS-based method for model parameter estimation. In order to overcome these problems, this paper proposes the novel DWRLS method which estimates separately the model fast and slow dynamics. SOC estimation is also achieved based on the ECM parameter estimation results, without the use of an additional full-order observer. Both the simulation and experimental studies have been conducted to validate the superiority of the proposed DWRLS method over the traditional LS algorithms in terms of modelling and state estimation accuracy. The results confirm convincingly that the proposed approach possesses enough capability for both offline model training, and online parameter and battery SOC estimation with high accuracy. This designed technique therefore has the high potential for realtime battery management applications in electric vehicles and other battery energy storage systems.

Acknowledgements

The research presented within this paper was undertaken as part of the ELEVATE project (EP/M009394/1) funded by the Engineering and Physical Sciences Research Council (EPSRC), in partnership with the WMG High Value Manufacturing (HVM) Catapult, funded by Innovate UK.

References

[1] Thackeray MM, Wolverton C, Isaacs ED. Electrical energy storage for transportation—approaching the limits of, and going beyond, lithium-ion batteries. Energy & Environ Sci 2012;5(7):7854–63.
[2] Divya K, Østergaard J. Battery energy storage technology for power systems—an overview. Electr Power Syst Res 2009;79(4):511–20.
[3] Zhang C, Li K, McLoone S, Yang Z. Battery modelling methods for electric vehicles-A review. In: European control conference (ECC). IEEE; 2014. p. 2673–8.
[4] Plett GL. Sigma-point Kalman filtering for battery management systems of LiPB-based HEV battery packs: Part 2: simultaneous state and parameter estimation. J power sources 2006;161(2):1369–84.
[5] Plett GL. Extended Kalman filtering for battery management systems of LiPB-based HEV battery packs: Part 3. State and parameter estimation. J Power sources 2004;134(2):277–92.
[6] Xia B, Chen C, Tian Y, Wang M, Sun W, Xu Z. State of charge estimation of lithium-ion batteries based on an improved parameter identification method. Energy 2015;90:1426–34.
[7] Bruen T, Marco J. Modelling and experimental evaluation of parallel connected lithium ion cells for an electric vehicle battery system. J Power Sources 2016;310:91–101.
[8] Pastor-Fernandez C, Bruen T, Widanage WD, Gama-Valdez M-A, Marco J. A study of cell-to-cell interactions and degradation in parallel strings: implications for the battery management system. J Power Sources 2016;329:574–85.
[9] Liu K, Li K, Yang Z, Zhang C, Deng J. An advanced Lithium-ion battery optimal charging strategy based on a coupled thermoelectric model. Electrochimica Acta 2017;225:330–44.
[10] Liu K, Li K, Zhang C. Constrained generalized predictive control of battery charging process based on a coupled thermoelectric model. J Power Sources 2017;347:145–58.
[11] Li Y, Wang C, Gong J. A combination Kalman filter approach for State of Charge

estimation of lithium-ion battery considering model uncertainty. Energy 2016;109:933–46.
[12] Widanage W, Barai A, Chouchelamane G, Uddin K, McGordon A, Marco J, et al. Design and use of multisine signals for Li-ion battery equivalent circuit modelling. Part 1: signal design. J Power Sources 2016;324:70–8.
[13] Widanage WD, Barai A, Chouchelamane GH, Uddin K, McGordon A, Marco J, et al. Design and use of multisine signals for Li-ion battery equivalent circuit modelling. Part 2: model estimation. J Power Sources 2016;324:61–9.
[14] Zhang C, Li K, Deng J, Song S. Improved realtime state-of-charge estimation of LiFePO4 battery based on a novel thermoelectric model. IEEE Trans Industrial Electron 2017;64(1):654–63.
[15] Zhao X, Cai Y, Yang L, Deng Z, Qiang J. State of charge estimation based on a new dual-polarization-resistance model for electric vehicles. Energy 2017;135:40–52. https://doi.org/10.1016/j.energy.2017.06.094. ISSN 0360-5442.
[16] Zheng F, Jiang J, Sun B, Zhang W, Pecht M. Temperature dependent power capability estimation of lithium-ion batteries for hybrid electric vehicles. Energy 2016;113:64–75.
[17] Chen M, Rincon-Mora GA. Accurate electrical battery model capable of predicting runtime and IV performance. IEEE Trans energy Convers 2006;21(2):504–11.
[18] Verbrugge M, Tate E. Adaptive state of charge algorithm for nickel metal hydride batteries including hysteresis phenomena. J Power Sources 2004;126(1):236–49.
[19] Verbrugge M. Adaptive, multi-parameter battery state estimator with optimized time-weighting factors. J Appl Electrochem 2007;37(5):605–16.
[20] Guo X, Kang L, Yao Y, Huang Z, Li W. Joint estimation of the electric vehicle power battery state of charge based on the least squares method and the kalman filter algorithm. Energies 2016;9(2):100.
[21] Rahimi-Eichi H, Baronti F, Chow M-Y. Online adaptive parameter identification and state-of-charge coestimation for lithium-polymer battery cells. IEEE Trans Industrial Electron 2014;61(4):2053–61.
[22] Xiong R, Sun F, Gong X, Gao C. A data-driven based adaptive state of charge estimator of lithium-ion polymer battery used in electric vehicles. Appl Energy 2014;113:1421–33.
[23] Zhang X, Wang Y, Yang D, Chen Z. An on-line estimation of battery pack parameters and state-of-charge using dual filters based on pack model. Energy 2016;115:219–29.
[24] Wei Z, Tseng KJ, Wai N, Lim TM, Skyllas-Kazacos M. Adaptive estimation of state of charge and capacity with online identified battery model for vanadium redox flow battery. J Power Sources 2016;332:389–98.
[25] Garnier H, Wang L, Young PC. Direct identification of continuous-time models from sampled data: issues, basic solutions and relevance. Identification of continuous-time models from sampled data. Springer; 2008. p. 1–29.
[26] Alaoui K, Chaplais F. Two time scale system identification: some asymptotic results. Proc European Control Conference, Netherlands. p. 1856–1861.
[27] Xia B, Zhao X, De Callafon R, Garnier H, Nguyen T, Mi C. Accurate Lithium-ion battery parameter estimation with continuous-time system identification methods. Appl Energy 2016;179:426–36.
[28] Zhang C, Marco J, Allafi W, Dinh T, Widanage WD. Online battery electric circuit model estimation on continuous-time domain using linear integral filter method. Proc World Acad Sci Eng Technol 2017;4(3):823.
[29] Hu Y, Wang YY. Two time-scaled battery model identification with application to battery state estimation. IEEE Trans Control Syst Technol 2015;23(3):1180–8.
[30] Dai H, Xu T, Zhu L, Wei X, Sun Z. Adaptive model parameter identification for large capacity Li-ion batteries on separated time scales. Appl Energy 2016;184:119–31.
[31] Wei Z, Lim TM, Skyllas-Kazacos M, Wai N, Tseng KJ. Online state of charge and model parameter co-estimation based on a novel multi-timescale estimator for vanadium redox flow battery. Appl Energy 2016;172:169–79.
[32] Barai A, Widanage WD, Marco J, McGordon A, Jennings P. A study of the open circuit voltage characterization technique and hysteresis assessment of lithium-ion cells. J Power Sources 2015;295:99–107.
[33] Zhang C, Li K, Pei L, Zhu C. An integrated approach for real-time model-based state-of-charge estimation of lithium-ion batteries. J Power Sources 2015;283:24–36.
[34] Chang M-H, Huang H-P, Chang S-W. A new state of charge estimation method for LiFePO4 battery packs used in robots. Energies 2013;6(4):2007–30.
[35] Ljung L. System identification (2nd ed.): theory for the user. Prentice-Hall, Inc; 1999.
[36] Ljung L, Söderström T. Theory Pract recursive Identif JSTOR. 1983.
[37] Garnier H, Mensler M, Richard A. Continuous-time model identification from sampled data: implementation issues and performance evaluation. Int J Control 2003;76(13):1337–57.
[38] Young P. Some observations on instrumental variable methods of time-series analysis. Int J Control 1976;23(5):593–612.
[39] Young P, Jakeman A. Refined instrumental variable methods of recursive time-series analysis Part I. Single input, single output systems. Int J Control 1979;29(1):1–30.
[40] Duong V-H, Bastawrous HA, Lim K, See KW, Zhang P, Dou SX. Online state of charge and model parameters estimation of the LiFePO4 battery in electric vehicles using multiple adaptive forgetting factors recursive least-squares. J Power Sources 2015;296:215–24.
[41] Wang T, Pei L, Wang T, Lu R, Zhu C. Capacity-loss diagnostic and life-time prediction in lithium-ion batteries: Part 1. Development of a capacity-loss diagnostic method based on open-circuit voltage analysis. J Power Sources 2016;301:187–93.
[42] Dubarry M, Truchot C, Liaw BY. Synthesize battery degradation modes via a diagnostic and prognostic model. J power sources 2012;219:204–16.